# Modeling high-resolution downhole pressure transducer to achieve semi-distributed measurement in oil and gas production wells

Leonardo B. M. Silva, [1], and Edval J. P. Santos[2]

[1] Department of Informatics, Instituto Federal de Alagoas, 57100-791, Rio Largo - AL, Brazil
[2] Laboratory for Devices and Nanostructures, Universidade Federal de Pernambuco, 50740-530, Recife-PE, Brasil.
e-mail: edval@ee.ufpe.br

***Abstract*— A full 3D computer model is developed to evaluate the performance impact of intrinsic loss and various geometrical features in high-resolution single-mode thickness-shear pressure transducer. The intrinsic loss is modeled as viscosity factors, which allows for a more efficient computer model. In this paper, the developed model is applied to get an insight in the evolution of high-resolution pressure transducer, from Hewlett-Packard™ to Quartzdyne™. As the quality factor is related to the inverse of the resolution, the transducing element optimization process to achieve the highest quality factor possible is investigated, considering the impact of crystal quality and geometrical features, such as: thickness, diameter and convexity (plano-convex and bi-convex). Temperature-dependent elastic constants are used to improve the model accuracy in modeling temperature effects on the vibrating resonator-type transducer. Boundary load conditions are used to simulate hydrostatic pressure. The simulations to extract the frequency shift are carried out in the range of $14$ psi ($96.5$ kPa) to $20000$ psi ($137.89$ MPa) and $0\,^{o}$C to $200\,^{o}$C for pressure and temperature, respectively, as such ranges are typically found in oil and gas wells. A miniaturization path to achieve semi-distributed measurement in oil and gas production wells is presented.**

***Index Terms*— Quality factor, piezoelectric transducer, pressure, temperature, quartz resonator, loss mechanism.**

## I. Introduction

High-resolution pressure and temperature measurements in oil and gas wells are performed with piezoelectric resonator-type transducers using materials such as: boron silicate (tourmaline), lanthanum gallium silicate (langasite), gallium orthophosphate, and quartz. In such applications, quartz is the standard material due to its sensitivity, frequency stability with respect to cut error, long-term stability, pressure and temperature cycling stability, and rugged characteristics. Gallium orthophosphate or langasite can be used in higher temperature range, as found in deeper oil wells. It is estimated that away from tectonic plates the borehole pressure increases at $24.5$ MPa per kilometer and the borehole temperature increases at $25\,^{o}$C per kilometer [1]. Resonator-type transducer resolution is related to the inverse of the quality factor, Q-factor. For pressure measurements, the achieved resolution is in parts per million, ppm. Thus, Q-factor greater than one million is standard. The state-of-the-art commercial sensor is based on the Quartzdyne™ transducer. The complete sensor, including transducer, conditioning and processing electronics and connector, is sealed in a stainless steel case and its length is over $500$ mm. It can be mounted in a structure on the welltop, named X-mas tree, as shown in Figure 1, for single-point measurement. Another mounting point is the well bottom, in which is deployed the permanent downhole gage.

Fig. 1 Sensor installation at the X-mas tree for oil well monitoring.

The collected data is used in well planning and safety, also for reservoir assessment or management. It allows for the estimation of reservoir permeability and oil/water interface for optimal well completion. Thus, the requirement of high quality factor is key for early detection of pressure buildup to monitor well stability during drilling, reservoir assessment and production phases. The most common geometry is the disk-like, with both sides partially covered with electrodes. Typically constructed as a single-mode thickness-shear disk resonator, such transducer is used for downhole pressure and temperature measurement in oil and gas wells for the last 50 years [1].

Since the first downhole transducer manufactured by Hewlett-Packard™, HP, there has been a continued size reduction process, see Table I. Smaller transducer dimensions

Digital Object Identifier 10.29292/jics.v14i2.25

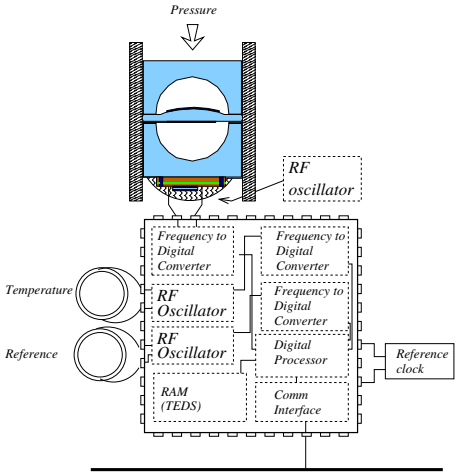


Fig. 2: Proposal of a smart high-resolution pressure sensor. To produce a miniaturized sensor capable of withstanding harsh conditions, the circuitry could be implemented with silicon-on-insulator, SOI, technology.

combined with proper packaging may help reducing costs, while improving its thermal transient response and alleviating possible dead-volume calibration problems. On the downside, less volume reduces the power handling capability. Another penalty is the reduction on the absolute accuracy. Most commercial transducers used in oil and gas applications are bulk resonators for single-point measurement. Semi-distributed or distributed measurement in oil and gas wells is an unsolved problem. A proposal for a smart high-resolution pressure sensor is presented in Figure 2. The extremely high Q-factor required makes micro-electro-mechanical systems (MEMS) based transducer not applicable for downhole measurements, as such high $Q$-factor is not achieved with present day technology [2, 3, 4, 5, 6].

A computer model is an important tool for the design of high performance transducers. With such model, the design can be optimized to achieve the highest quality factor possible while considering the impact of crystal quality and geometrical features, such as: thickness, diameter and convexity (plano-convex and bi-convex). Due to the anisotropic nature of quartz (trigonal symmetry), it is necessary to have a full 3D FEM based model for quartz resonators based pressure transducers for accurate Q-factor estimations. Besides, full 3D FEM based model allows for the evaluation of non-symmetric 3D geometries. Besides, the resonance frequency is highly dependent on crystal orientation (cut angle). Commercially, the AT-cut quartz crystal is the selected cut due to its lower thermal sensitivity, which allows for the production of stable high-resolution resonator-type pressure transducers. It is also a valuable tool to understand the evolution of high-resolution downhole pressure transducer, from Hewlett-Packard™to Quartzdyne™ [1, 4].

Proper understanding and modeling of the various dissipation mechanisms is extremely important, as they have a direct impact on the transducer $Q$-factor, which can be estimated directly from vibration analysis by taking into consideration the material dissipation. Additionally, the presence of the mounting support reduces the $Q$-factor, as it works as an energy sink. The effect of the mounting support can be modeled with a supporting structure in which all of the waves transmitted into it are dissipated, and none of the incoming waves on the boundary interface are reflected back to the resonator. This approximation is also applied in the remaining lateral border. The semi-infinite energy sink is realized by a resonator (source) - to - base (sink) boundary interface that is perfectly radiating to the waves from the source: the interface is transparent to the source waves, i.e., there are no reflections at the interface. The modeling of the semi-infinite energy sink is performed by applying a scaled boundary finite element method. The reflections are limited by the application of the perfectly matched layer (PML) technique, which absorbs the outgoing wave energy. This lower bound $Q$-factor is useful for evaluating the resonator design and the mounting support. This technique is known as the semi-infinite energy sink method for predicting the lower bound $Q$-factor [7, 8].

In this work, the aim is to present a computer model which can be used to investigate the size reduction process occurred in the last decades while keeping the Q-factor above $10^6$ for the single-mode thickness-shear resonator geometry. Previously, a simplified implementation of the model was discussed [9, 10]. This paper is divided into four sections. This introduction is the first. Next, the energy loss mechanisms and the computer model construction are presented in the materials and methods section. The results and analysis are in the third section. Finally, the conclusions.

## II. Materials and Methods

The HP™/Quartzdyne™ resonator geometry is selected to demonstrate the 3D-FEM model performance. This geometry is used in state-of-the-art X-mas tree or downhole transducers. As presented in Table I, the HP transducer uses the BT-cut, and the Quartzdyne transducer uses the AT-cut. In this paper, the dual-mode, thickness-shear quartz pressure transducer is not analysed, as it represents a different geometry class [11, 12]. The developed model is used to evaluate the influence of intrinsic loss of quartz and various geometrical features on the resonator Q-factor values, and its response to changing temperature and hydrostatic pressure. For this work, the AT-cut is used, but the model can be easily modified to evaluate any crystaline materials or crystal cuts. The steps carried out in model construction and validation are as follows.

- Energy loss mechanisms assessment.
- Computer model construction.
- Model validation.
  - Quality factor vs. frequency, $Q \times f$.
  - Quality factor vs. cross-section curvature, $Q \times h_c$.
  - Relative frequency variation vs. temperature, $\frac{\Delta f}{f} \times T$.
  - Relative frequency variation vs. pressure, $\frac{\Delta f}{f} \times p$.
- Transducer design optimization.

Table I. Pressure transducer dimension evolution.

| **Manufacturer** | **Dimensions** ($\Phi \times$L) | **Max. Pressure** (MPa) | **Resolution** (Pa) | **Cut** | **Year** |
|---|---|---|---|---|---|
| *Hewlett-Packard*™ | $25.4\,\text{mm} \times 86.4\,\text{mm}$ | 75 | 69 | BT | 1970 |
| *Halliburton*™ | $18.3\,\text{mm} \times 48.3\,\text{mm}$ | 110 | $< 70$ | AT | 1988 |
| *Quartzdyne*™ | $14.7\,\text{mm} \times 15.2\,\text{mm}$ | 110 | 23 | AT | 1993 |

By applying the newly constructed model, and considering the best crystal quality, the transducing element can be evaluated with respect to geometrical features, such as: thickness, diameter and convexity (plano-convex and biconvex), to achieve the highest quality factor possible.

Oil wells are getting deeper, thus transducers and circuitry have to withstand higher temperatures and pressures. It is estimated that away from tectonic plates the downhole temperature increases at $25\,^{o}$C per kilometer and the hydrostatic pressure increases at $24.5\,$MPa per kilometer [1]. The transducing element should be able to withstand pressures greater than $20000\,$psi ($137.89\,$MPa) at temperatures of $200\,^{o}$C, while keeping the $Q$-factor over $10^6$. Besides, such requirements should have the lowest impact on the fabrication complexity.

For temperature simulations, temperature-dependent elastic constants, from $0\,^{o}$C to $200\,^{o}$C, are used. Experimentally, it is found that a third-order polynomial is enough to model temperature effects on the elastic constants [13]. Other temperature constants values can be found in [14]. As for pressure simulations, a boundary load condition is used to get the pressure-induced frequency shift, in the range of $14\,$psi ($96.5\,$kPa) to $20000\,$psi ($137.89\,$MPa). To simulate the pressure induced frequency shift, only the first order elastic constant is used, as the non-linear behavior is expected to be negligible in the pressure range evaluated [15].

### *A. Energy loss mechanisms assessment*

The energy loss mechanisms are classified in two main groups: losses in the crystal itself, classified as intrinsic losses, or losses due to the construction of the resonator and the environment, classified as extrinsic losses. Some losses are unavoidable and others can be minimized [8, 16].

Intrinsic mechanisms include:

- Thermoelastic dissipation.
- Dissipation due to phonon-phonon interactions.
- Dissipation due to lattice defects.

Extrinsic mechanisms include:

- Friction loss via interaction with ambient gases.
- Loss due to electrode resistance.
- Friction loss at the electrode-quartz interface.
- Loss due to surface roughness.
- Leakage towards the mounting support.
- Excitation of undesirable modes.

The detailed mathematical analysis of the various loss mechanisms is an extremely complex problem, thus resulting in extremely long computation time. However, a simpler mathematical model can be implemented considering the loss mechanisms as a viscous phenomenon [8, 17]. This is specially useful for the internal loss mechanisms. Thus, the constitutive relations of piezoelectricity can be modified as presented in Equations 1-3. The constant values for quartz are presented in Table II.

$$T_{ij} = c_{ijkl} S_{kl} - e_{ijk} E_k + (\eta_{ijkl} \dot{S}_{kl}) \quad (1)$$

$$D_i = e_{ijk} S_{jk} + \varepsilon_{ij} E_j \quad (2)$$

$$J_i = \sigma_{ik} E_k \quad (3)$$

in which, $T_{ij}$ is the $ij$ component of the stress tensor, $S_{kl}$, $S_{jk}$ are components of the strain tensor, $\dot{S}_{kl}$ is the time variation of the component of the strain tensor, $E_k$, $E_j$ are components of the electric field vector, $D_i$ is the $i$ component of the electric displacement vector, $c_{ijkl}$ is the component of the elasticity or elastic stiffness matrix, $e_{ijk}$ is component of the piezoelectric coupling matrix, $\varepsilon_{ij}$ is the electric permittivity matrix, $J_i$ is the component of the current density vector, and $\sigma_{ik}$ is the component of the electric conductivity.

The coefficients $\eta_{ijkl}$, in the term in parenthesis in Equation 1, represent the viscosity of quartz, corresponding to the internal friction in the piezoelectric material. This simplification allows for a more efficient computer model [7, 8]. Equation 3 accommodates the loss attributed to resistivity. Next, to include the impact of the extrinsic losses on the Q-factor, the transducer geometry is designed with a computer software.

Different materials can be used as piezoelectric transducer, such as: boron silicate (tourmaline), lanthanum gallium silicate (langasite), gallium orthophosphate, and quartz. In oil and gas applications, the AT-cut quartz crystal is the selected cut due to its lower thermal dependence, frequency stability with respect to cut error, and long term stability. Typical parameters for the AT-cut quartz parameters are presented in Table III. For this crystal cut, the vibration mode used is the thickness-shear. The quality factor, Q-factor, is inversely related to the loss mechanisms, which can be classified in two main groups: intrinsic and extrinsic. Considering intrinsic losses only, the Q-factor decreases as frequency increases, as shown in the following expression for the Q-factor [17].

$$Q = \frac{\bar{c}_{66}}{\omega \eta_{66}} \quad (4)$$

in which,

$$\bar{c}_{66} = c_{66} \left(1 + k_{26}^2\right) \ , \quad k_{26}^2 = \frac{e_{26}^2}{c_{66} \varepsilon_{22}}, \quad (5)$$

Table II. Elastic, piezoelectric, dielectric constants for right-handed quartz. The $\theta$ angle is counterclockwise oriented.

$$[c] = \begin{bmatrix} 86.74 & 6.99 & 11.91 & 17.91 & 0 & 0 \\ 6.99 & 86.74 & 11.91 & -17.91 & 0 & 0 \\ 11.91 & 11.91 & 107.2 & 0 & 0 & 0 \\ 17.91 & -17.91 & 0 & 57.94 & 0 & 0 \\ 0 & 0 & 0 & 0 & 57.94 & 17.91 \\ 0 & 0 & 0 & 0 & 17.91 & 39.88 \end{bmatrix} \times 10^9 \text{ N/m}^2$$

$$[e] = \begin{bmatrix} -17.1 & 17.1 & 0 & 4.06 & 0 & 0 \\ 0 & 0 & 0 & 0 & -4.06 & 17.1 \\ 0 & 0 & 0 & 0 & 0 & 0 \end{bmatrix} \times 10^{-2} \text{ C/m}^2$$

$$[\varepsilon] = \begin{bmatrix} 39.21 & 0 & 0 \\ 0 & 39.21 & 0 \\ 0 & 0 & 41.03 \end{bmatrix} \times 10^{-12} \text{ C/Vm}$$

$\omega$ is the angular frequency, and $\eta_{66}$ is the viscosity. The Voigt notation is applied.

Using the AT-cut quartz parameters presented in Table III, one can obtain a numerical expression, which can be used as part of model validation process [17, 18].

$$Q = 14.54 \times 10^{12} \times f^{-1} \tag{6}$$

in which, the frequency, $f$, is in Hz.

Table III.: Typical parameters for AT-cut quartz crystal. The Voigt notation is applied.

| Quartz parameter | Value |
|---|---|
| $c_{66}$ (N/m$^2$) | $29.01 \times 10^9$ |
| $e_{26}$ (C/m$^2$) | $-9.5 \times 10^{-2}$ |
| $\varepsilon_{22}$ (C/Vm) | $39.82 \times 10^{-12}$ |
| $\eta_{66}$ (Pa $\cdot$ s) | $0.32 \times 10^{-3}$ |
| $\sigma_{22}$ ($(\Omega \cdot$ m$)^{-1}$) | $0.005 \times 10^{-12}$ |
| $\rho$ (kg/m$^3$) | 2649 |

### B. Computer model construction

The model is implemented in COMSOL Multiphysics software [19]. But details are given for implementation of the model with other platforms. The steps are as follows: geometry design, material selection (cut angle), mesh generation, absorbing regions, and physics (solid mechanics and electrostatics). First the plano-plano geometry is used to validate the procedure, and next different profiles are examined, namely: plano-convex and bi-convex.

*Geometry design:*

The disk-shaped plano-plano geometry is selected for validating the procedure, because it is very close to the geometry used in the industry for many applications. Due to the anisotropic (trigonal symmetry) nature of quartz, a full 3D FEM based model is used to accurately estimate the Q-factor. Besides, the full 3D model allows for the evaluation of non-symmetric 3D geometries. A cross-sectional view is presented in Figure 3. The dimensions of the disk are based on the Quartzdyne pressure resonator, that has a 3rd

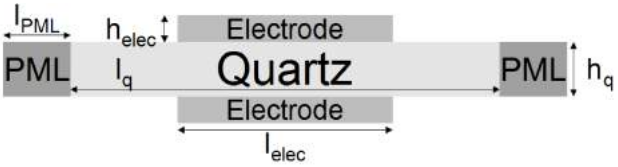


Fig. 3: Cross-sectional view of the disk-shaped resonator geometry with electrodes on both sides.

OT resonance frequency at 7.22 MHz [4]. For this simulation, the same frequency was analyzed in the first harmonic, so the disk thickness is $h_q = 230\,\mu$m and the diameter is $l_q = 15$ mm. Thus, differently from the Quartzdyne transducer, the first harmonic is used. There is no loss, as far as model validation is concerned. Of course, to manufacture the transducer, it is best to use the third harmonic, allowing for a thicker plate. The electrode thickness is $h_{elec} = 100$ nm and diameter is $l_{elec} = 0.5 \times l_q$. As the electrode is an ideal conductor, the thickness is modeled as a single layer. The PML region is explained later.

*Material selection:*

Next, a material has to be defined for each region. The electrodes are ideal equipotentials: ideal conductors with no atomic mass. For the simulation, it was defined as an ideal metal. In real transducers, gold is used. For the quartz crystal region shown in Figure 3, the material properties are orientation dependent. In this work, the right-handed quartz crystal is used. For each crystal cut, there is a set of constants for the elastic stiffness matrix, piezoelectric coupling matrix and relative permittivity matrix. For the 3D simulation, one can enter the matrix elements for the chosen cut or use the general matrix, and perform the crystal cut rotation directly in the software tool using Euler angles. The crystallographic orientation adopted in the simulations are based on the 1987 IEEE standard, in which the AT-cut is defined as (*YXl*)-35.25° [20]. The selected software tool follows such convention [21]. Both, the COMSOL library and published elastic constants are used to carry out the simulations [13].

*Mesh generation:*

For the thickness-shear mode, the mesh density in the thickness direction directly influences the correct simulation

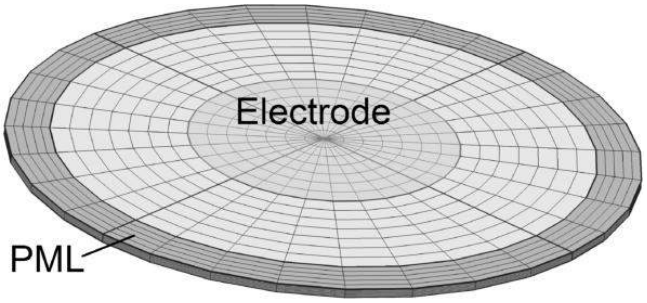


Fig. 4: Mesh used in the simulations. The darker region around the border is the PML domain and the disk on top represents the electrode domain. $l_q = 15mm$, $h_q = 230\mu$m, $l_{PML} = 1.2$ mm, $l_{elec} = 0.5 \times l_q$ and $h_{elec} = 100$ nm.

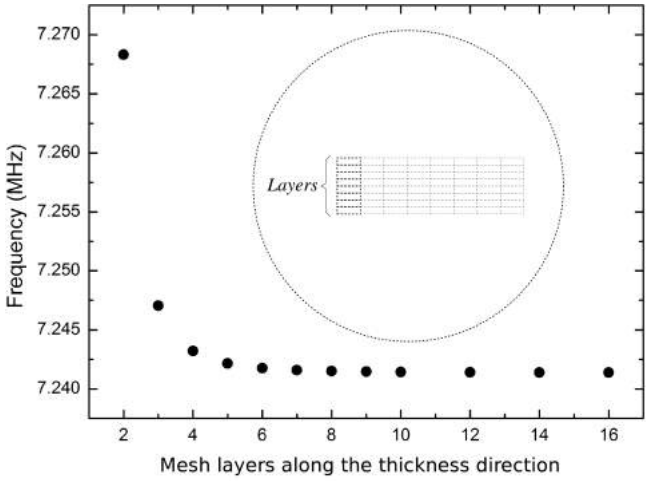


Fig. 5: The resonance frequency should not be influenced by the number of mesh elements. Simulating the resonance frequency as a function of the number of layers along the thickness direction yields that an 8-element mesh by half-wavelength is a good compromise between computation time and accuracy.

of the resonance frequency. However, one should be careful at increasing the mesh density, as it increases the computation time. An evaluation of the fundamental frequency value as a function of the number of mesh elements along the thickness direction is presented in Figure 5. From the simulation results there is a good compromise at the density of 8 mesh elements by half-wavelength. For the electrodes, only one layer in the thickness direction is considered sufficient, as the electrode conductivity is much higher as compared to the crystal. The generated mesh, presented in Figure 4, has 8 elements in the perpendicular direction, 32 elements in the azimuth and 23 elements in the radial direction, yielding 5888 elements. This is a trade-off, as increasing the number of element, increases the resolution, but also increases the computation time. With more computing power, more mesh elements can be used, including higher order mesh.

*Absorbing regions:*

To complete the plano-plano geometry, it is necessary to introduce a special region. For this purpose, the perfectly matched layer, PML, technique is applied. The PML region is an ideal absorbing domain. This allows a more realistic modeling of the resonator loss, as the PML region can be assumed to model the mounting support loss for this simpler geometry used to validate the model. All energy reaching the PML region is absorbed, none is reflected. This energy sink allows for obtaining a lower bound for the Q-factor, as it assumes that all energy reaching the mounting support is lost. Without the PML region, the reflected energy would bounce inside the structure yielding an unrealistic Q-factor. A PML region is not a boundary condition. The region specified as PML works as a semi-infinite ideal energy sink, it dissipates all the incident wave energy [7, 8, 22].

In COMSOL Multiphysics, PML is available for frequency response and eigenfrequency analysis. The material properties of the PML have to be the same as its adjacent domain. In Figure 4 a PML domain circumvents the disk resonator. The radius of the outer circle is not critical as long as it allows for the meshing requirements of the PML region, which is 5 - 6 mesh elements across.

*Physics:*

At this step, one defines the set of differential equations to be solved and its boundary conditions. In the piezoelectric region, COMSOL Multiphysics software solves both structural and electrical equations. In the electrode region, only the structural equation is solved. The electrical equations are not solved in the metallic region because an ideal metal is assumed, hence the electrodes can be approximated as an equipotential region. The dominant electromechanical coupling is exhibited by the piezoelectric region only.

Finally, one specifies the electrical and mechanical boundary conditions. One example of boundary condition is the electrode voltage level. In this work, one electrode is defined to be at 5 V, and the other is connected to the ground potential. For pressure simulations, one can use two types: fixed constraint, and boundary load. The fixed surface constraint is applied in some simulations to model a structure which is in a fixed position. The boundary load is a condition that replaces the standard free condition, it states that a given mechanical load is applied onto the boundary.

## III. Results and analysis

Both mechanical and electrical losses are introduced by means of loss factors, which are related to the viscosity. The viscosity matrix for quartz crystal at 30 $^o$C [18] is used. After introducing the loss mechanisms, the eigenfrequencies become complex. As a generalization of Equation 4, the real part is the actual modal frequency, and the imaginary part is related to the damping effect.

$$\text{loss factor} = \frac{\omega \cdot \eta_{ij}}{c_{ij}} \tag{7}$$

in which, $\omega$ is the angular frequency, $\eta_{ij}$ are the viscosity matrix elements, and $c_{ij}$ are the elastic constants, Voigt notation is used.

For model validation with the plano-plano geometry, the PML regions are used to model anchor or mounting support loss. Such regions (domains) absorb the elastic waves and contribute to the damping. The structural loss factor represents the hysteresis in a stress-strain curve and the dielectric loss factor represents the polarization loss, which manifests itself as the hysteresis in the polarization versus electric field curve of the material. The dielectric loss factor is required by the COMSOL software to carry out the simulation. The default zero-value is used. In this simulation, the dielectric

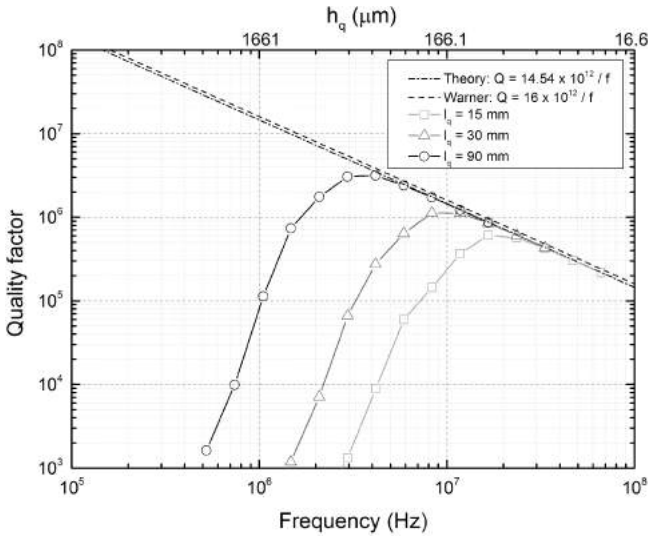


Fig. 6: Quality factor vs. frequency for the disk-shaped plano-plano quartz resonator with 15 mm, 30 mm and 90 mm in diameter ($l_q$), $l_{elec} = 0.5 \times l_q$, $l_{PML} = 1.2$ mm.

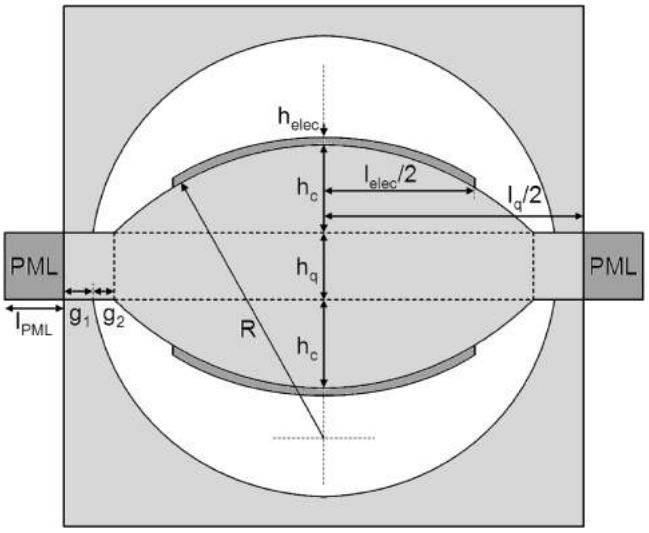


Fig. 7: Cross-section view of a complete pressure transducer with a bi-convex quartz resonator with caps.

loss is included in the viscosity loss factor. The electrodes are assumed loss-less.

A simulation involving mechanical boundary conditions such as these must be carried out in two steps: stationary, and eigenfrequency. At each step, geometrically nonlinear analysis is enabled.

### A. *Model validation with plano-plano geometry*

As a key validation for the constructed computer model, the first simulation performed is to extract the dependence of the Q-factor as a function of the resonance frequency, $f$, as this is a figure of merit for resonators [23, 24, 25, 26, 27]. This allows for comparison of the model with available data [23]. In this simulation, the electrode thickness is zero. Thus the electrode material is introduced because it is required by the interface. The frequency range is obtained for different diameters of the quartz disk: 15 mm, 30 mm and 90 mm in diameter. The results are presented in Figure 6.

It can be seen from Figure 6 that the Q-factor increases with frequency, reaches a maximum, and starts decreasing, as is observed experimentally. At high frequencies, the transducer Q-factor is limited by intrinsic losses.

According to available experimental data [23], the Q-factor limit due to intrinsic losses is given by $Q = 16 \times 10^{12} \times f^{-1}$. This is very close to the result in Equation 6, which is also extracted from the plot in Figure 6. The reduction of the Q-factor at lower frequencies is also observed experimentally [23]. This can be understood as caused by extrinsic losses, which is a function of the energy removed out from the transducer through the interfaces. Keeping the diameter fixed, a thicker disk causes more energy to be lost to the environment, and mounting structures, causing a reduction of the Q-factor at such frequency range.

### B. *Other geometries*

Next the model is used to evaluate the impact of different geometrical profiles in the Q-factor. It is expected that by using a convex surface the vibration energy can be confined, thus increasing the Q-factor. The convex surface reduces the acoustic energy reaching the transducer borders, and reduces undesired vibration modes. Different types of curvatures can be utilized, such as: plano-convex and bi-convex [28, 29]. First, a spherically-contoured surface is used, as shown in Figure 7. The convex shape can be manufactured by ultrasound machining, convex lapping and polishing, and for small geometries MEMS fabrication techniques can be applied [30, 31]. The radius, $R$, can be calculated as follows,

$$R = \frac{h_c}{2} + \frac{\left(\frac{l_q}{2} - g_1 - g_2\right)^2}{2h_c}. \tag{8}$$

in which, $h_c$ is the thickness of the curved surface at the center.

For the simulation, the electrodes thickness is set to zero, $l_q = 15$ mm, $h_q = 230\,\mu$m, $l_{elec} = 0.5 \times l_q$ and $l_{PML} = 1.2$ mm and $g_1 = g_2 = 0.8$ mm. Eigenfrequency analysis, by varying the geometric parameter $h_c$, are carried out to extract the Q-factor of the disk-shaped resonator with different surface convexities. The results for four types of curvature: bi-spheric, plano-spheric, plano-parabolic and plano-elliptic without caps and zero-thickness electrodes are shown in Figure 8. As expected the Q-factor increases with the curvature, the bi-convex shape displays higher Q-factor than any of the plano-convex shapes, as can be observed in Figure 8. However, by using just one convex surface is enough to concentrate the acoustic energy. This result is important because it simplifies the manufacturing process. Thus, the plano-convex shape is the best compromise, as the lapping and polishing procedure is easier to be performed at one side.

### C. *Temperature sensitivity*

The behavior of the resonance frequency shift as a function of temperature and cut angle around the AT-cut can be modeled as a third order polynomial [13], as shown in Equation 9. The frequency shift is calculated as $(f - f_0)/f_0$, in which $f$ is the measured frequency and $f_0$ is the frequency at the reference temperature. Considering the temperature-dependent equations for the elastic constants, and applying the values of the elastic constants for the Y-cut at 25 $^o$C,

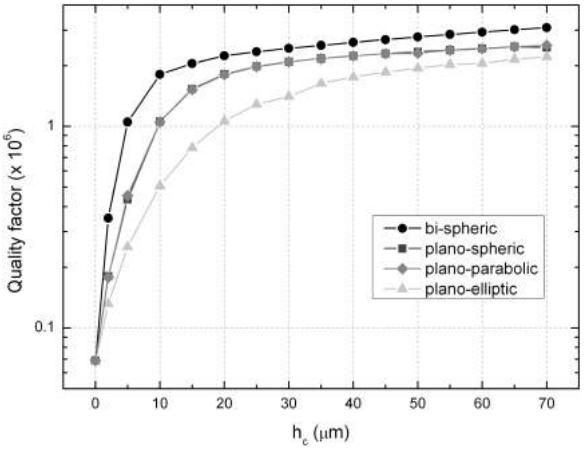


Fig. 8: Q-factor as function of the geometric parameter $h_c$ for the disk-shaped resonator with PML. The electrodes thickness is set to zero, $l_q = 15\,\text{mm}$, $h_q = 230\,\mu\text{m}$, $l_{elec} = 0.5 \times l_q$ and $l_{PML} = 1.2\,\text{mm}$ and $g_1 = g_2 = 0.8\,\text{mm}$. The plano-spheric and the plano-parabolic plots are almost perfectly superimposed.

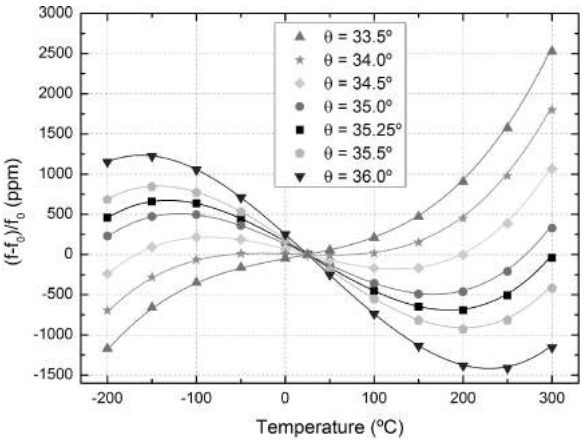


Fig. 9: Frequency shift as a function of the temperature for the disk-shaped in AT-cut quartz resonator. Each curve is normalized to the resonance frequency at $25\,^o\text{C}$. The continuous lines reproduce the behavior of the Mason's Equation. $l_q = 15\,\text{mm}$, $l_{elec} = 0.5 \times l_q$ and $h_q = 230\,\mu\text{m}$.

$50\,^o\text{C}$, $100\,^o\text{C}$ and $200\,^o\text{C}$, as given in Table IV [13, 32], one can perform a rotation using Euler angles to get the elastic constant for the AT-cut.

$$c_{pq}(T) = c_{pq}(T_0)\left[1 + \sum_{n=1}^{n=3} K_{pq}^n \times (T - T_0)^n\right] \qquad (9)$$

The frequency shift as a function of temperature for the disk-shaped resonator is obtained with the developed model. Using the plano-plano geometry presented in Figure 4, and considering $T = 25\,^o\text{C}$ as the reference temperature, the normalized resonance frequency of the first harmonic is plotted in parts per million. The result is presented in Figure 9. For this simulation, the Mason temperature constants are used [13]. Other constants can be easily implemented [14].

### *D. Pressure and temperature effects*

The combined response of the resonance frequency as a function of hydrostatic pressure and its temperature sensitivity is obtained for the plano-plano geometry with caps. It is the transducer shown in Figure 7 with $h_c = 0$. This is

Table IV.: Quartz elastic constants as a function of the temperature for the Y-cut.

| $c_{pq}$ | ($\times 10^9\,\text{N/m}^2$) | | | | |
|---|---|---|---|---|---|
| | J. Yang | W. Mason [13] | | | |
| | [32] | $25\,^o\text{C}$ | $50\,^o\text{C}$ | $100\,^o\text{C}$ | $200\,^o\text{C}$ |
| $c_{11}$ | 86.74 | 86.86 | 86.75 | 86.5 | 85.9 |
| $c_{12}$ | 6.99 | 6.6 | 6.15 | 5.19 | 3.18 |
| $c_{13}$ | 11.91 | 9.71 | 9.6 | 9.3 | 8.45 |
| $c_{14}$ | 17.91 | 18.15 | 18.2 | 18.26 | 18.29 |
| $c_{33}$ | 107.2 | 105.2 | 104.8 | 103.88 | 101.62 |
| $c_{44}$ | 57.94 | 58.82 | 58.58 | 58.04 | 56.78 |
| $c_{66}$ | 39.88 | 40.09 | 40.26 | 40.59 | 41.24 |

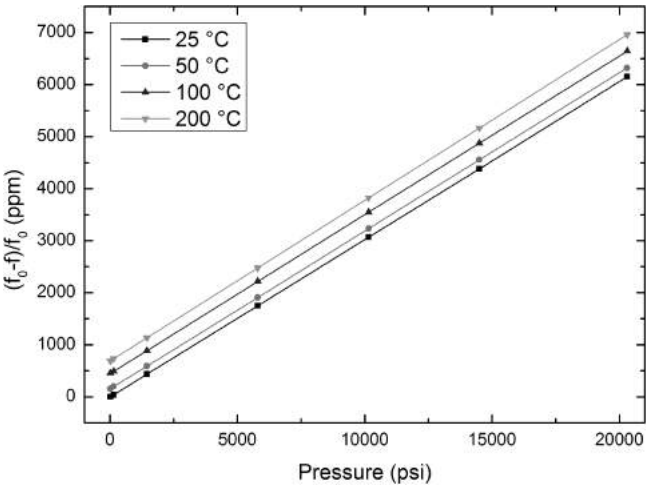


Fig. 10: Frequency shift as function of the pressure and temperature of $25\,^o\text{C}$, $50\,^o\text{C}$, $100\,^o\text{C}$ and $200\,^o\text{C}$. $l_q = 15\,\text{mm}$, $l_{elec} = 0.5 \times l_q$, $h_q = 230\,\mu\text{m}$ and $h_{elec} = 100\,\text{nm}$ for the plano-plano geometry.

equivalent to the Quartzdyne transducer, which is the state-of-the-art used in the oil and gas industry. The simulations were carried out in the temperature range from $25\,^o\text{C}$ to $200\,^o\text{C}$ and pressures from $14.7\,\text{psi}$ ($96.5\,\text{kPa}$) to $20000\,\text{psi}$ ($137.89\,\text{MPa}$). The results obtained are shown in Table V with $l_q = 15\,\text{mm}$, $l_{elec} = 0.5 \times l_q$, $h_q = 230\,\mu\text{m}$ and $h_{elec} = 100\,\text{nm}$. The behavior of the frequency shift in parts per million as function of the temperature and pressure is shown in Figure 10, in which the frequency at $25\,^o\text{C}$ and $14.7\,\text{psi}$ ($96.5\,\text{kPa}$) is used to normalize the data.

For a given isotherm, the pressure response appears fairly linear. In fact, these results show a good agreement with previous simulation results, which used the Nonlinear Stressed Homogeneous Temperature (NSHT) algorithm developed by Beerwinkle *et al* [33].

Considering state-of-the-art transducers, to allow for semi-distributed measurement in such harsh conditions, the transducing crystal should be integrated with a high-temperature silicon-on-insulator, SOI, chip, replacing alumina printed circuit board commmonly used, as shown in the proposed smart high-resolution pressure sensor presented in Figure 2. The SOI chip with RF oscillator, converter, data processing and communications, could be attached to the bottom of the pressure transducer with the temperature and reference transducers mounted next to it. The tranducers are part of a Pierce RF oscillator connected to a frequency to digital converter [34]. To save energy, an energy management module could be included. Besides, results in Figure 8

Table V.: Resonance frequencies for different pressures and temperatures of the Quartzdyne-type structure sensor.

| Pressure | | Frequency (MHz) | | |
|---|---|---|---|---|
| ($N/m^2$) | (psi) | 25 $^oC$ | 100 $^oC$ | 200 $^oC$ |
| $1.01 \times 10^5$ | 14.7 | 7.257514 | 7.254224 | 7.252512 |
| $1.0 \times 10^6$ | 145 | 7.257237 | 7.253941 | 7.252186 |
| $1.0 \times 10^7$ | 1450 | 7.254335 | 7.251091 | 7.249280 |
| $4.0 \times 10^7$ | 5803 | 7.244827 | 7.241421 | 7.239549 |
| $7.0 \times 10^7$ | 10155 | 7.235239 | 7.231748 | 7.229750 |
| $1.0 \times 10^8$ | 14507 | 7.225727 | 7.222141 | 7.220030 |
| $1.4 \times 10^8$ | 20310 | 7.212869 | 7.209297 | 7.207002 |

suggests that the transducing element could be further miniaturized. A possible target for the miniaturized transducer and electronics is to fit a stainless steel package with $\Phi = 10\,\text{mm}$ diameter and about $L = 100\,\text{mm}$ of length. Although, the system should still use wired communications and energy source. The new sensor could be mounted in the mandrel at fixed positions in the well tubing to achieve semi-distributed measurement [35].

## IV. Conclusions

A 3D-FEM computer model for the AT-cut quartz plate, which takes into account the intrinsic and extrinsic loss mechanisms, is constructed and implemented. For calculation efficiency, the simplifying assumption of modeling the losses as friction factors is used. The right-handed AT-cut quartz crystal is selected as the reference material. The developed model can be easily modified to evaluate other crystaline materials or crystal cuts. Details are given such as the model can be implemented in different multiphysics software tools.

The model is validated for the AT-cut quartz crystal by extracting the $Q \times f$ curve, by evaluating $Q$ as a function of the cross-section profile, by extracting the relative frequency shift as a function of temperature, and by extracting the relative frequency shift for the disk-shaped transducer as a function of the hydrostatic pressure. The geometry is the same as the HP™ or Quartzdyne™ transducers. To compare with published data, the dimensions used are the same as the Quartzdyne transducer, except for the plate thickness. Differently from the Quartzdyne transducer, the first harmonic is used. The quartzdyne transducer is manufactured to oscillate at the third harmonic. There is no loss, as far as model validation is concerned. Of course, to manufacture the transducer, it is best to use the third harmonic, allowing for a thicker plate. The simulated results reproduce the behavior of the AT-cut Quartzdyne transducer as found in the literature, and the general trends imposed by theoretical arguments.

To speed up the simulation, the electrodes are zero-thickness ideal conductors. A reduction of the Q-factor is expected, due to the conductivity and atomic number of the material used in the electrodes. Typically gold is the material of choice. The PML region is included to model the absorbed energy in the mounting clips, yielding a lower bound for the $Q$-factor.

The model offers an insight in the evolution of high-resolution pressure transducer, as it allows an evaluation of the impact of geometrical features to achieve the highest quality factor possible. Considering the limit imposed by intrinsic loss at high frequencies, bi-convex and plano-convex disk surfaces can be used to increase the quality factor substantially. A small curvature already yields a factor of ten increase. Furthermore, the plano-convex disk resonator presents almost the same quality factor as the bi-convex. Hence, the plano-convex is the best compromise, as the manufacturing process is simpler. The Q-factor as a function of frequency of a downhole quartz sensor, capable of withstanding pressures greater than $20000\,\text{psi}$ ($137.89\,\text{MPa}$) at temperatures of $200\,^oC$ has been simulated. A possible miniaturization route is to bond an SOI-based circuitry directly onto the backside of the transducer capsule.

## Acknowledgments

The authors thank Eng. Maurício Galassi for many fruitful discussions, PETROBRAS, Brazilian oil company, CNPq and FINEP, Brazilian agencies, for their support.

## References

[1] B. K. Sinha, M. S. Patel, *Recent Developments in High Precision Quartz and Langasite Pressure Sensors for High Temperature and High Pressure Applications*,IEEE International Frequency Control Symposium (IFCS), pp. 1–13, 2016.

[2] N. Matsumoto, Y. Sudo, B. K. Sinha, M. Niwa, *Long-term stability and performance characteristics of crystal quartz gauge at high pressures and temperatures*, *Ultrasonics, Ferroelectrics and Frequency Control, IEEE Transactions on*, vol. 47, no. 2, pp. 346–354, 2000.

[3] L. Spassov, V. Gadjanova, R. Velcheva, B. Dulmet, *Short-and long-term stability of resonant quartz temperature sensors*, *Ultrasonics, Ferroelectrics and Frequency Control, IEEE Transactions on*, vol. 55, no. 7, pp. 1626–1631, 2008.

[4] R. W. Ward, R. B. Wiggin, *Quartz pressure transducer technologies*, Quartzdyne, Inc. www.quartzdyne.com/pdfs/techqptt.pdf (1997).

[5] S. M. B. Goutham, R. Kirikera, W. Patton, *Modeling thickness shear mode quartz sensors for increased downhole pressure & temperature applications*, *Proceedings of the COMSOL Conference 2010 Boston*, 2010.

[6] P. Krempl, G. Schleinzer, W. Wallnöfer, *Gallium phosphate, $GaPO_4$: a new piezoelectric crystal material for high-temperature sensorics*, Sensors and Actuators A, 61, 361-363, 1997.

[7] Y. Yook-Kong, M. S. Patel, M. Tanaka, *Estimation of quartz resonator Q and other figures of merit by an energy sink method*, *Ultrasonics, Ferroelectrics and Frequency Control, IEEE Transactions on*, vol. 54, no. 7, pp. 1386–1398, 2007.

[8] Y.-K. Yong, M. S. Patel, M. Tanaka, *Theory and experimental verifications of the resonator Q and equivalent electrical parameters due to viscoelastic and mounting supports losses*, *Ultrasonics, Ferroelectrics and Frequency Control, IEEE Transactions on*, vol. 57, no. 8, pp. 1831–1839, 2010.

[9] L. B. M. Silva, E. J. P. Santos, *Quartz transducer modeling for development of BAW resonators*, *Proceedings of the COMSOL Conference 2012 Milan*, 2012.

[10] ——, *Modeling quality factor in AT-cut quartz-Crystal resonators*, in *Proceedings of the SBMICRO 2013 Curitiba-Brasil*, 2013.

[11] R. J. Besson, J. J. Boy, B. Glotin, Y. Jinzaki, B. K. Sinha, M. Valdois, *A dual-mode thickness-shear quartz pressure sensor*, IEEE Trans. Ultrasonics, Ferroelectrics, and Frequency Control, **40(5)**, pp. 584-591, 1993.

[12] M. S. Patel, B. K. Sinha, *A dual-mode thickness-shear quartz pressure sensor for high pressure applications*, IEEE Sensors Journal, **18(12)**, pp. 4893-4901, 2018.

[13] W. Mason, *Zero Temperature Coefficient Quartz Crystals for Very High Temperatures*, *Bell System Tech. J*, vol. 30, pp. 366–380, 1951.

[14] A. Ballato, *Basic Material Quartz and Related Innovations*. In: Piezoelectricity. Springer Series in Materials Science, vol 114. Springer, Berlin, Heidelberg (2008).

[15] E. Calderon, M. Gauthier, F. Decremps, G. Hamel, G. Syfosse, A. Polian, *Complete determination of the elastic moduli of $\alpha$-quartz under hydrostatic pressure up to 1 GPa: an ultrasonic study*, J. Phys.: Condens. Matter Vol. 19, 436228 (2007).

[16] A. Rampal, *Experimental and theoretical study of quartz and InP piezoelectric MEMS resonators*, 2010.

[17] A. Arnau, *Piezoelectric Transducers and Applications*, Springer Verlag, 2008.

[18] J. Lamb, J. Richter, *Anisotropic acoustic attenuation with new measurements for quartz at room temperatures*, *Proceedings of the Royal Society of London. Series A. Mathematical and Physical Sciences*, vol. 293, no. 1435, pp. 479–492, 1966.

[19] COMSOL Multiphysics FEM software v. 4.4, *http://www.comsol.com*.

[20] *IEEE Standards on Piezoelectricity ANSI/IEEE Standard No. 176-1987*, 1987.

[21] COMSOL documentation, *Thickness Shear Mode Quartz Oscillator*, *http://www.comsol.com*.

[22] P. Steeneken, J. Ruigrok, S. Kang, J. Van Beek, J. Bontemps, and J. Koning, *Parameter extraction and support-loss in MEMS Resonators*, in *COMSOL Users Conference 2007*, 2007.

[23] A. W. Warner, *Design and performance of ultraprecise 2.5-Mc quartz crystal units*, *Bell Syst. Tech. J*, vol. 39, no. 9, pp. 1193–1217, 1960.

[24] R. C. Smythe, *Material and resonator properties of langasite and langatate: a progress report*, in *Frequency Control Symposium, 1998. Proceedings of the 1998 IEEE International*. IEEE, 1998, pp. 761–765.

[25] F. Watanabe, T. Watanabe, *Convex quartz crystal resonator of extremely high Q in 10 MHz-50 MHz*, in *Ultrasonics Symposium, 2002. Proceedings. 2002 IEEE*, vol. 1. IEEE, 2002, pp. 1007–1010.

[26] J. R. Vig, F. L. Walls, *A review of sensor sensitivity and stability*, in *Frequency Control Symposium and Exhibition, 2000. Proceedings of the 2000 IEEE/EIA International*. IEEE, 2000, pp. 30–33.

[27] Y.-K. Yong, M. Patel, J. Vig, A. Ballato, *Effects of electromagnetic radiation on the Q of quartz resonators*, *Ultrasonics, Ferroelectrics and Frequency Control, IEEE Transactions on*, vol. 56, no. 2, pp. 353–360, 2009.

[28] N. Matsumoto, T. Yamate, B. Sinha, S. Sato, A. F. Veneruso, J. Lawrence, Y. Barriol, S. Daito, *Pressure transducer*, July 2 2007, US Patent App. 11/772, 244.

[29] B. K. Sinha, *Doubly rotated contoured quartz resonators*, *Ultrasonics, Ferroelectrics and Frequency Control, IEEE Transactions on*, vol. 48, no. 5, pp. 1162–1180, 2001.

[30] P. Nussbaum, R. Völkel, H. P. Herzig, M. Eisner, S. Haselbeck, *Design, fabrication and testing of microlens arrays for sensors and microsystems*, Pure Appl. Opt. vol. 6, 617 (1997).

[31] L. Li, K. Ishii, Y. Tsutsui, S. Shoji, J. Mizuno, *Development of roll press UV imprint process for replication of micro lens array on the large and thin quartz substrate*, 7th IEEE International Conference on Nano/Micro Engineered and Molecular Systems (NEMS), 27-30 (2012).

[32] J. Yang, *Analysis of piezoelectric devices*, World Scientific Pub Co Inc, 2006.

[33] A. D. Beerwinkle, R. P. Singh, G. R. Kirikera, *Simulating Frequency Nonlinearities in Quartz Resonators at High Temperature and Pressure*, in *Proceedings of the COMSOL Conference Boston*, 2011.

[34] Edval J. P. Santos, Leonardo B. M. Silva, *FPGA-Based Smart Sensor Implementation with Precise Frequency to Digital Converter for Flow Measurement*. In: VI Southern Programmable Logic Conference, 2010, Ipojuca (Porto de Galinhas). Proceedings of the VI Southern Programmable Logic Conference. Piscataway (EUA): Institute of Electrical and Electronics Engineers - IEEE, 2010. p. 21-26.

[35] L. B. M. Silva, *Miniaturização de sensores piezoelétricos para medição de pressão elevada com alta resolução em ambientes agressivos*. Doctoral dissertation. Universidade Federal de Pernambuco, Recife (2014).